THE JOURNAL OF BIOLOGICAL CHEMISTRY VOL. 288, NO. 48, pp. 34428–34442, November 29, 2013

Identifying Key Amino Acid Residues That Affect α-Conotoxin AuIB Inhibition of α3β4 Nicotinic Acetylcholine Receptors*

Received for publication, August 30, 2013, and in revised form, October 4, 2013 Published, JBC Papers in Press, October 7, 2013, DOI 10.1074/jbc.M113.512582

Anton A. Grishin[‡1,2], Hartmut Cuny[‡1], Andrew Hung[‡1], Richard J. Clark[§1,3], Andreas Brust[§], Kalyana Akondi[§], Paul F. Alewood[§], David J. Craik[§4], and David J. Adams[‡5]

From the [‡]Health Innovations Research Institute, RMIT University, Melbourne, Victoria 3083, Australia and the [§]Institute for Molecular Bioscience, The University of Queensland, Brisbane, Queensland 4072, Australia

Background: α-Conotoxin AuIB interacts with α3β4 nAChRs and $GABA_B$ receptors, but structural determinants of these interactions are unknown.
Results: Using alanine scanning mutagenesis and molecular dynamics, we identified residues crucial for AuIB·α3β4 nAChR interaction.
Conclusion: We identified the key residues that mediate AuIB·α3β4 nAChR interaction.
Significance: Ability to direct α-conotoxin binding to nAChRs or $GABA_B$ receptors will improve analgesic conopeptides.

α-Conotoxin AuIB is a selective α3β4 nicotinic acetylcholine receptor (nAChR) subtype inhibitor. Its analgesic properties are believed to result from it activating $GABA_B$ receptors and subsequently inhibiting $Ca_V2.2$ voltage-gated calcium channels. The structural determinants that mediate diverging AuIB activity at these targets are unknown. We performed alanine scanning mutagenesis of AuIB and α3β4 nAChR, homology modeling, and molecular dynamics simulations to identify the structural determinants of the AuIB·α3β4 nAChR interaction. Two alanine-substituted AuIB analogues, [P6A]AuIB and [F9A]AuIB, did not inhibit the α3β4 nAChR. NMR and CD spectroscopy studies demonstrated that [F9A]AuIB retains its native globular structure, so its activity loss is probably due to loss of specific toxin-receptor residue pairwise contacts. Compared with AuIB, the concentration-response curve for inhibition of α3β4 by [F9A]AuIB shifted rightward more than 10-fold, and its subtype selectivity profile changed. Homology modeling and molecular dynamics simulations suggest that Phe-9 of AuIB interacts with a two-residue binding pocket on the β4 nAChR subunit. This hypothesis was confirmed by site-directed mutagenesis of the β4-Trp-59 and β4-Lys-61 residues of loop D, which form a putative binding pocket. AuIB analogues with Phe-9 substitutions corroborated the finding of a binding pocket on the β4 subunit and gave further insight into how AuIB Phe-9 interacts with the β4 subunit. In summary, we identified critical residues that mediate interactions between AuIB and its cognate nAChR subtype. These findings might help improve the design of analgesic conopeptides that selectively "avoid" nAChR receptors while targeting receptors involved with nociception.

Peptides isolated from the venom of cone snails belonging to the genus *Conus* are valuable pharmacological tools, and some are also promising drug leads (1–5). α-Conotoxins are a subfamily of these peptides and consist of 12–19 amino acid residues, including four cysteines with a characteristic CC-C-C arrangement (type I cysteine framework) (6, 7). These four cysteines can yield three possible disulfide connectivities: globular (I-III, II-IV), ribbon (I-IV, II-III), and beads (I-II, III-IV). However, naturally occurring α-conotoxins typically exhibit the "globular" conformation (7). The number of amino acids in each of the two loops between the framework cysteine residues is used to divide α-conotoxins into subclasses. For example those with four amino acids in loop 1 and six in loop 2 are referred to as 4/6-α-conotoxins.

Nicotinic acetylcholine receptors (nAChRs)[6] are transmembrane proteins that form cationic ligand-gated channels that mediate fast excitatory cholinergic neurotransmission in the central nervous system (CNS). They also have an important regulatory role in the body, modulating the release of several neurotransmitters. The importance of nAChRs is emphasized by their involvement in various CNS disorders, including Alzheimer disease, schizophrenia, pain, nicotine addiction, and cancer (8–11).

nAChRs belong to the Cys-loop family of ligand-gated ion channels that is characterized by a pentameric composition and subunit arrangement in the receptor (12, 13). Seventeen nAChR subunits have been identified (12). Six of them are muscle nAChR subtypes (α1β1δγ or α1β1εγ) found exclusively at neuromuscular junctions, whereas the rest (α2-α10, β2-β4) can combine in numerous homomeric (having only α subunits) or heteromeric (having α and β subunits) neuronal nAChR sub-

* This work was supported by National Health and Medical Research Council Program Grant 569927 and Australian Research Council Discovery Grant DP 1093115.
[1] These authors contributed equally to this work.
[2] Present address: Bionomics Ltd., Thebarton, SA 5031, Australia.
[3] An Australian Research Council Future Fellow. Present address: School of Biomedical Sciences, The University of Queensland, Brisbane, QLD 4072, Australia.
[4] A National Health and Medical Research Council Professorial Fellow.
[5] An Australian Research Council Australian Professorial Fellow. To whom correspondence should be addressed: Health Innovations Research Institute, RMIT University, P.O. Box 71, Bundoora, Victoria 3083, Australia. Tel.: 61-3-9925-6606; E-mail: david.adams@rmit.edu.au.

[6] The abbreviations used are: nAChR, nicotinic acetylcholine (ACh) receptor; TOCSY, total correlation spectroscopy; AChBP, acetylcholine binding protein; MD, molecular dynamics; NAL, 3-(2-naphthyl)L-alanine; TrpD, tryptophan of loop D.

types (8). Heteromeric receptor subtypes exhibit two distinct subunit stoichiometries of α:β ratios (2:3 or 3:2) and display different pharmacological properties (11, 14). The diversity of neuronal heteromeric nAChR subtypes *in vivo* increases even further when more than one α/β subunit is included within the same pentamer (*e.g.* α3β2β4 or α3α6β2) (11).

AuIB is a 4/6-α-conotoxin isolated from the venom of *Conus aulicus* and consists of 15 amino acid residues (15). In contrast with most α-conotoxins that inhibit 2–3 nAChR subtypes with similar potency, AuIB only inhibits the α3β4 nAChR subtype and with micromolar potency (15). Two other α-conotoxins, BuIA, an unusual 4/4-α-conotoxin isolated from the venom of *Conus bullatus*, and the recently described 4/7-α-conotoxin RegIIA from *Conus regius*, have been found to be considerably more potent inhibitors of the α3β4 subtype, blocking it at low nanomolar concentrations (16, 17). However, unlike AuIB, BuIA and RegIIA are not selective for the α3β4 subtype but potently block other nAChR subtypes too. Additionally, despite α-conotoxins generally being described as competitive nAChR antagonists (18–20), AuIB is a non-competitive α3β4 antagonist (14).

α-Conotoxins with a different disulfide bond connectivity from the native form typically show losses in biological activity. However, the ribbon disulfide isomer (I-IV, II-III) of AuIB retains its nAChR inhibition with greater potency than that of the native globular (I-III, II-IV) AuIB disulfide isomer in rat parasympathetic ganglion neurons (21). Furthermore, the AuIB ribbon isomer exhibits stoichiometry-dependent blockade of oocyte-expressed α3β4 nAChRs, and unlike globular AuIB, it competitively inhibits the α3β4 nAChR (14).

Interestingly, AuIB and several other α-conotoxins (*e.g.* RgIA and Vc1.1) exhibit analgesic properties when tested in animal models of pain (22–24). These conotoxins inhibit various nAChR subtypes (α3β4, α9α10, and α7), but all inhibit high voltage-activated calcium channels via G protein-coupled $GABA_B$ receptor activation with much more potency than their corresponding nAChR target (25–27). Therefore, $GABA_B$ receptor-mediated suppression of N-type calcium channels ($Ca_V2.2$) has been suggested as the common mechanism of their analgesic action (28).

To design more effective α-conotoxin analogues that could lead to improved analgesic drugs with fewer side effects, it is important to know the structural determinants of inhibition at nAChRs and $GABA_B$ receptors. This would help us focus on analgesic activity and remove the undesired side effects in engineered α-conotoxin analogues. Furthermore, it might help to identify previously overlooked naturally occurring analgesic conotoxins. Here we take the first step toward this goal by characterizing the residues that are critical for α-conotoxin AuIB inhibition of α3β4 nAChRs. We show that the interaction between phenylalanine (Phe) at position 9 of AuIB and β4-Tyr-59–β4-Lys-61 of the loop D on the (–) face of the β4 subunit are essential for this inhibition. A preliminary report of these results in part has been presented in abstract form (29).

EXPERIMENTAL PROCEDURES

Peptide Synthesis—All peptides were assembled on MBHA-Rink-Amide resin (Novabiochem) by solid-phase peptide synthesis using a Liberty Microwave Peptide Synthesizer with the *in situ* activation/*N*,*N*,*N*′,*N*′-tetramethyl-*O*-(1*H*-benzotriazol-1-yl)uranium hexafluorophosphate protocol and Fmoc (*N*-(9-fluorenyl)methoxycarbonyl) chemistry (30). Cys-3 and Cys-15 were incorporated into the peptide chain with acetamidomethyl side chain protection during assembly to facilitate regioselective disulfide formation. Peptides were cleaved from the resin using trifluoroacetic acid (TFA) with tri-isopropylsilane and water as scavengers (9:0.5:0.5 (v/v) TFA:tri-isopropylsilane:water) at 22 °C for 2 h. The TFA was then removed under vacuum, and peptides were precipitated with ether, filtered, dissolved in 50% acetonitrile containing 0.05% TFA, and lyophilized. Crude peptides were purified by reversed-phase high performance liquid chromatography (RP-HPLC) on a C_{18} column using a gradient of 0–80% B (A, H_2O, 0.05% TFA; B, 90% CH_3CN, 10% H_2O, 0.045% TFA) in 80 min. Analytical RP-HPLC and electrospray mass spectrometry confirmed the purity and molecular mass of synthesized peptides.

The first disulfide bond in each peptide was formed by incubating peptides in 0.1 M NH_4HCO_3 (pH 8.2, 0.3 mg/ml) overnight at 22 °C, then purifying them by RP-HPLC. The second disulfide bond was formed by incubating peptides with iodine in acidic conditions. Peptides were dissolved in 50% aqueous acetic acid (0.5 mg/ml). To this solution 100 μl of 1 M HCl/mg of peptide was added, then a solution of 0.1 M I_2 in 50% acetic acid was slowly added until the solution became pale yellow. The reaction mixture was stirred for 12 h at 22 °C in the dark. The reaction was quenched by adding 1 M ascorbic acid until the mixture became colorless. The peptide was purified by RP-HPLC, and fractions were combined after analytical RP-HPLC confirmed purity. Electrospray mass spectrometry was used to confirm the peptide identity.

Nuclear Magnetic Resonance (NMR) and Circular Dichroism (CD)—NMR spectra for all AuIB analogues were recorded on samples dissolved in 90% H_2O and 10% D_2O at a pH of ~4. Bruker Avance 500 and 600 MHz NMR spectrometers were used to acquire spectra, including ^1H, total correlation spectroscopy (TOCSY) and nuclear Overhauser effect spectroscopy (NOESY) data, as described previously (18, 31), and processed using Topspin (Bruker). All spectra were recorded at 290 K, and chemical shifts were referenced to the residual water signal at 4.85 ppm. Processed spectra were analyzed and assigned within the program Sparky (32).

For CD spectroscopy experiments, 70 μM concentrations of each peptide were dissolved in 20 mM sodium phosphate buffer at pH 7. To examine the helical propensity of each isomer, CD data were also obtained for each product after 30% tetrafluoroethene was added to the solution. Spectra were acquired on a Jasco J-810 spectropolarimeter, which was routinely calibrated using 0.6% (w/v) ammonium-D-camphor-10-sulfonate. All experiments were conducted at room temperature (21–23 °C) under a nitrogen atmosphere (15 ml/min). The experimental parameters were set to a scanning speed of 50 nm/min, response time of 1 s, sensitivity range of 100 millidegrees, and a step resolution of 1 nm. Absorbance was measured in the far UV region (185–260 nm) using a 1-mm path length quartz cuvette. Each recording was an accumulation of four scans. To eliminate any possible interference from the solvent, cuvette,

and spectropolarimeter optics, we subtracted CD spectra of the pure solvents from each sample.

Protein Sequence Alignment—The National Institute of Health's online Constraint-based Multiple Alignment Tool, COBALT (www.ncbi.nlm.nih.gov), was used to align protein sequence, and conservative domains were taken into account. Residues of nAChR subunits were numbered according to the sequences of the mature proteins that lacked the signal peptide at the start of their sequences.

Site-directed Mutagenesis of α3 and β4 nAChR Subunits—Constructs in which Trp-59, Lys-61, or both β4 nAChR residues were substituted by alanine ([W59A]β4, [K61A]β4, and [W59A]+[K61A]β4, respectively) were generated using the Geneart Site-directed Mutagenesis System (Invitrogen catalog no. A13282) and the following primers: 5′-cat gac cac cag cat cgc gct gaa aca gga atg gac tga cta cc-3′ and 5′-ggt agt cag tcc att cct gtt tca gcg cga tgc tgg tgg tca tg-3′ for [W59A]β4; 5′-cat gac cac cag cat ctg gct ggc aca gga atg gac tga cta cc-3′ and 5′-ggt agt cag tcc att cct gtg cca gcc aga tgc tgg tgg tca tg-3′ for [K61A]β4; 5′-cat gac cac cag cat cgc gct ggc aca gga atg gac tga cta cc-3′ and 5′-ggt agt cag tcc att cct gtg cca gcg cga tgc tgg tgg tca tg-3′ for [W59A]+[K61A]β4. Gln-198 of the α3 subunit was substituted to alanine ([Q198A]α3) in the same way using primers 5′-ctg tga gga gat cta cgc aga cat cac gta ctc gc-3′ and 5′-gcg agt acg tga tgt ctg cgt aga tct cct cac ag-3′. All point mutations were confirmed by sequencing.

cRNA Preparation—Plasmid DNAs encoding rat α3, α4, α9, α10, β2, and β4 nAChR subunits and human α7 nAChR subunits were obtained from Dr. J. Patrick, Baylor College of Medicine, Houston TX, Dr. J. Lindstrom University of Pennsylvania, Philadelphia PA, and OriGene Technologies Inc., Rockville MD. The plasmids were linearized with appropriate restriction enzymes, and cRNA was synthesized *in vitro* using a SP6 or T7 *in vitro* transcription kit (mMessage mMachine; Ambion, Foster City, CA). RNA for different nAChR subunits to be co-injected into the same oocytes was synthesized in parallel on the same day using identical procedures to maximize the consistency of concentration and purity between subunits.

Oocyte Preparation and Microinjection—Stage V-VI oocytes were obtained from *Xenopus laevis*, defolliculated with collagenase (Type I, Sigma) at 3 mg/ml, and incubated at 18 °C in sterile ND96 solution (96 mM NaCl, 2 mM KCl, 1.8 mM $CaCl_2$, 1 mM $MgCl_2$, and 5 mM HEPES at pH 7.5) supplemented with 50 μg/liter gentamycin (Sigma). Glass pipettes for microinjection were pulled from glass capillaries (3–000-203 GX, Drummond Scientific Co.). The cRNAs were diluted in water to the appropriate concentrations (~0.1 ng/nl), and 5 ng of RNA was injected into each oocyte using a microinjector (Nanojet, Drummond Scientific Co.). Electrophysiological recordings were carried out 2–7 days after microinjection.

Electrophysiological Recordings and Data Analysis—Two-electrode voltage clamp recordings from oocytes were carried out at room temperature using a GeneClamp 500B amplifier (Molecular Devices Corp., Sunnyvale, CA) at a holding potential of −80 mV. The voltage-recording and current-injecting electrodes were pulled from borosilicate glass (GC150T-15, Harvard Apparatus Ltd.) and had resistances of 0.3–1.5 megaohms when filled with 3 M KCl. Oocytes were continuously perfused in a recording chamber with a volume of ~50 μl, with ND96 solution at 2 ml/min, applied by a gravity-fed perfusion system. nAChR-mediated currents were evoked by pipetting 100 μl of acetylcholine (ACh) into the bath when the perfusion was temporarily halted. ACh concentration was 50 μM unless specified otherwise. Oocytes were preincubated with the peptide for ~5 min, then ACh and the peptide were co-applied. Peak ACh-evoked current amplitude was recorded before and after peptide incubation using pClamp 9 software (Molecular Devices). The effects of native AuIB and its peptide analogues on ACh-evoked nAChR-mediated currents were defined as peak current amplitudes relative to the average peak current amplitude of 3–5 control ACh applications, recorded before preincubation with the peptides. Concentration-response curves for AuIB and [F9A]AuIB were fitted by unweighted nonlinear regression to the logistic equation,

$$E_x = E_{max} X^{nH} / (X^{nH} + IC_{50}{}^{nH}) \quad \text{(Eq. 1)}$$

where E_x is the response, X is the peptide concentration, E_{max} is the maximal response, nH is the slope factor (Hill slope), and IC_{50} is the peptide concentration that gives 50% inhibition of the maximal response. All electrophysiological data were pooled (n = 3–6 for each data point) and represent the arithmetic means ± S.E. of the mean. One-way analysis of variance followed by Bonferroni's post hoc test was used to compare current amplitudes affected by AuIB analogues with those of the native peptide. Data were statistically analyzed using SigmaPlot Version 11.0 (Systat Software Inc., San Jose, CA) or Prism5 (GraphPad Software Inc., La Jolla, CA).

Molecular Modeling and Docking Simulation—Homology models of the extracellular ligand binding domain of the rat $(\alpha3)_2(\beta4)_3$ nAChR bound to AuIB, [F9A]AuIB, or [F9Y]AuIB were constructed using the crystallographic coordinates of *Aplysia californica* acetylcholine-binding protein (AChBP) co-crystallized with the double mutant α-conotoxin PnIA[A10L,D14K] (Protein Data Bank accession code 2BR8) as a template. This template was chosen to provide a suitable 4/7 α-conotoxin-bound conformation of the receptor for subsequent molecular dynamics (MD) simulations and analyses.

AuIB and mutant peptides were modeled bound to the two α3(+)β4(−) receptor binding sites using the geometry of the PnIA mutant in the AChBP crystal structure as a template. Rat α3 and β4 sequences were obtained from the Swiss-Prot database (codes P04757 and P12392, respectively) and aligned with the template sequence using the ClustalW server. BLOSUM was used as the scoring matrix. With the multiple alignment as input, 10 AuIB·α3β4, [F9A]AuIB·α3β4, and [F9Y]AuIB·α3β4 complex models were generated using Modeler9v6. The top-ranking models were selected and validated using PROCHECK. MD simulations were carried out on the top models of both receptor complexes.

MD Simulations—Before MD simulations, the energies of the complexes were minimized using the steepest descent algorithm and an energy gradient convergence criterion of 0.01 kcal/mol/Å. Each receptor complex was placed in icosahedral simulation boxes with edge lengths of 100 × 100 × 100 Å and solvated with 34,000 TIP3P water molecules. To neutralize charge and pro-

vide a salt concentration of ~150 mM, 94 Na^+ and 70 Cl^- ions were added to the solvent. All simulations were performed using GROMACS Version 4.5 (75) with the CHARMM27 forcefield (with cmap) (76, 77). All subsequent simulations were performed using a constant particle number, pressure, and temperature ensemble. Temperature was maintained at 300 K using the Nose-Hoover temperature coupling algorithm, and pressure was maintained at 1 atm using Berendsen's pressure coupling algorithm. Time steps of 2 fs were used to integrate all simulations. Solvent equilibration simulations of 100 ps lengths were performed. The non-hydrogen atoms of the receptor and peptides were positionally restrained so the solvent and ions could relax from an initially semi-crystalline structure. "Data collection" simulations of both complexes were then conducted, and all atoms of the system were free to undergo dynamics. Each complex was simulated for 100 ns. All analyses were performed on the final 20 ns of the trajectories to reduce bias from initial homology model conformations. Molecular graphics were produced using VMD Version 1.9.2 (78). All analyses were done using a combination of VMD, GROMACS analysis software suite, and in-house scripts.

RESULTS

Alanine Scanning Mutagenesis Identifies Residues in the AuIB Sequence That Are Critical for Its Interaction with the α3β4 nAChR Subtype—To find residues in the AuIB sequence that contribute most to α3β4 nAChR inhibition, we performed alanine scanning mutagenesis of the peptide. We systematically substituted each of the original residues to alanine, except for the four cysteines essential for maintaining the peptide globular structure and the native alanine at position 10 (see Fig. 1, *A* and *B*). All peptides were successfully synthesized using solid-phase peptide synthesis and a regioselective approach to form disulfide bonds to produce the globular disulfide framework. For future reference, we refer to globular AuIB as native AuIB. Each alanine mutant structure was analyzed using NMR and CD spectroscopy. The NMR spectral data for each peptide except [P6A]AuIB were successfully assigned whereby αH_i–NH_{i+1} NOE connectivities observed in NOESY spectra were used in the sequential assignment of the individual spin systems determined from TOCSY spectra.

The [P6A]AuIB mutant exhibited broadened signals and multiple conformations in the TOCSY and NOESY spectra, so could not be assigned. The loss of secondary structure in the [P6A]AuIB mutant was confirmed by CD spectroscopy (Fig. 1*C*). Pro-6 is the only highly conserved amino acid residue in α-conotoxins apart from the cysteines and is responsible for helix initiation by inducing the 3_{10} helix turn in the peptide backbone (33, 34). Mutation of Pro-6 to alanine has also been shown to disrupt the α-conotoxin Vc1.1 structure (35).

Secondary αH chemical shifts represent the difference between an observed αH chemical shift and that of the corresponding residue in a random coil peptide. They are strong indicators of the presence of a secondary structure (36). Secondary shift analysis of the chemical shift data indicated that, for native AuIB and analogues [G1A]AuIB, [S4A]AuIB, [P7A]AuIB, [F9A]AuIB, [T11A]AuIB, [P13A]AuIB and [D14A]AuIB, residues 6–10 have negative αH secondary shifts (Fig. 1*D*). These negative αH secondary shifts indicate a helical region, which is consistent with the previously reported three-dimensional structure of native AuIB (21) and other α-conotoxin structures reported to date (37). Interestingly, NMR secondary shift data for [Y5A]AuIB and [N12A]AuIB were more consistent with the ribbon isomer of AuIB (21) despite using a regioselective disulfide bond formation strategy to form the native (globular) isomer (Fig. 1*D*). This was confirmed by CD spectroscopy (Fig. 1*C*).

The effect of point modifications in the AuIB analogues on α3β4 nAChR-mediated current inhibition was examined by two-electrode voltage clamp recordings in oocytes expressing the α3β4 nAChR subtype. The relative amount of inhibition AuIB alanine-substituted analogues produced was compared with that of non-modified peptides at a fixed concentration (3 μM; ~ IC_{50} AuIB (14)) (Fig. 2, *A* and *B*).

Only three residues in the AuIB sequence significantly reduced inhibition of relative peak ACh-evoked current amplitude when alanine was substituted for them. These were Gly-1 (0.82 ± 0.11, $n = 3$; $p < 0.05$), Pro-6 (1.02 ± 0.07, $n = 3$; $p < 0.001$), and Phe-9 (1.07 ± 0.15, $n = 3$; $p < 0.001$) compared with a relative peak current amplitude of 0.51 ± 0.07 ($n = 6$) obtained in the presence of native AuIB (Fig. 2*B*). Interestingly, Gly1 replacement by Ala reduced α3β4 nAChR inhibition, although Gly1 does not belong to either loop 1 or loop 2 of AuIB, which are thought to be the primary mediators of α-conotoxin interaction with nAChRs (6, 7). Unlike the [G1A]AuIB mutation, which retained minor inhibitory activity, P6A and F9A analogues exhibited a complete loss of inhibitory activity. As the NMR and CD data showed that secondary structure of [P6A]AuIB is irregular (Fig. 1, *C* and *D*), we concluded that this peptide's loss of inhibitory activity was due to disruption in the three-dimensional structure. This is not surprising, as Pro-6 is believed to be responsible for inducing the 3_{10} helix turn in the backbone of α-conotoxins (33, 34). In contrast, [F9A]AuIB NMR and CD spectrum data were consistent with the native AuIB structure (Fig. 1, *C* and *D*). This led us to conclude that the F9A substitution is specific and relevant to the peptide-receptor interaction rather than a general disruption of the peptide structure.

Characterization of [F9A]AuIB Inhibition of the α3β4 nAChR Subtype—Our next step was to probe the degree to which [F9A]AuIB inhibitory activity is impaired by modifying the Ala to Phe substitution. Because the [F9A]AuIB analog was not active at ~IC_{50} concentration of the native AuIB (3 μM) (Fig. 2*A*), we tested this analog at higher concentrations, up to the highest practical concentration available (30 μM). The [F9A]AuIB analog applied at 10 μM mildly inhibited ACh-evoked currents, with the amplitude reduced to 0.77 ± 0.04 ($n = 4$) of normalized control currents (Fig. 3, *A* and *B*). This indicates that Phe to Ala substitution at position 9 of AuIB may strongly reduce the affinity of the modified peptide for α3β4 nAChRs but does not disrupt peptide-receptor interaction altogether. However, native AuIB completely blocked the current at this concentration (0.05 ± 0.01, $n = 6$) (Fig. 3, *A* and *B*). A concentration of 30 μM [F9A]AuIB inhibited 55% of current amplitude (0.45 ± 0.07, $n = 3$). The resulting concentration-response curve demonstrates a rightward shift, indicating

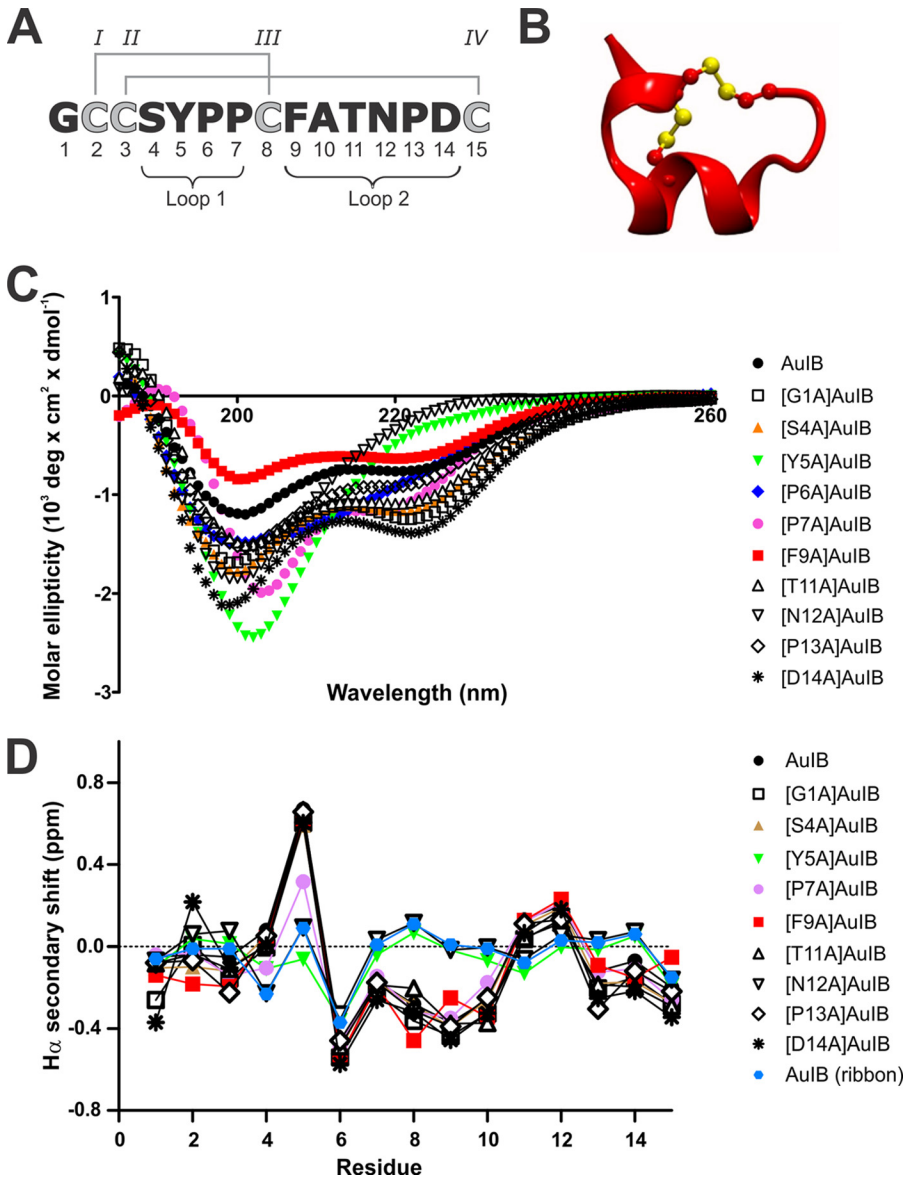

FIGURE 1. **Characteristics of AuIB and its analogues.** *A*, sequence of amino acid residues in α-conopeptide AuIB. The disulfide bonding pattern characteristic to the native AuIB globular isoform is indicated above the sequence: $^{2}CCX_{4}C^{8}$ (*I–III*) and $^{3}CX_{4}CX_{6}C^{15}$ (*II–IV*). The residues between cysteines $^{3}CX_{4}C^{8}$ and $^{8}CX_{6}C^{15}$ form the peptide loop 1 and loop 2, respectively. *B*, three-dimensional visualization of the AuIB structure (Protein Data Bank accession code 1MXN). Note that the second longer loop folds in an α-helical structure. *C*, CD spectra of Ala analogues compared with those of native globular AuIB revealed that [G1A]AuIB (*open squares*), [S4A]AuIB (*orange triangles*), [P7A]AuIB (*purple circles*), [F9A]AuIB (*red squares*), [T11A]AuIB (*open triangles*), [P13A]AuIB (*open diamonds*), and [D14A]AuIB (*asterisks*) analogues have similar spectra to globular AuIB (*black circles*). [Y5A]AuIB (*inverted green triangles*), [P6A]AuIB (*blue diamonds*), and [N12A]AuIB (*inverted open triangles*) analogues lack the α-helix characteristic CD absorption and show a single peak in the spectrum only, indicating their secondary structure is disrupted. *D*, NMR secondary shift analysis of the α-conotoxin AuIB Ala analogues. The shift values of [G1A]AuIB, [S4A]AuIB, [P7A]AuIB, [F9A]AuIB, [T11A]AuIB, [P13A]AuIB, and [D14A]AuIB compared with native globular AuIB (*black circles*) highlight the similarity in values across the full length of the peptide and confirm the secondary structure of these mutated peptides is well preserved. A series of negative values observed from residues 6–10 indicates there is a helical secondary structure in this region of the peptides, which is consistent with the three-dimensional structure of native globular AuIB. The [Y5A]AuIB and [N12A]AuIB analogues had αH secondary shift values consistent with the ribbon isomer of AuIB (*blue hexagons*).

[F9A]AuIB interaction with α3β4 nAChRs is markedly reduced (Fig. 3*B*).

The Selectivity Profile of [F9A]AuIB for nAChR Subtypes—Previously, most α-conotoxins that act on neuronal nAChRs were shown to have only relative selectivity in the sense that they inhibit two to three nAChR subtypes with similar potency and rarely inhibit just one nAChR subtype (6, 7). To date, AuIB is the only α-conotoxin shown to selectively inhibit the α3β4 nAChR subtype (15). As described above, substituting Phe-9 to Ala in AuIB led to complete loss in activity at α3β4. We also assessed the pharmacological profile of [F9A]AuIB at other nAChR subtypes. When tested, [F9A]AuIB (3 μM) exhibited only 16.2% inhibition of relative current amplitude (0.84 ± 0.1, $n = 3$) at α3β2 nAChRs, whereas no activity was observed at α4β4 nAChRs ($n = 5$) (Fig. 4*A*). However, we found that 3 μM [F9A]AuIB produced minor potentiation at the homomeric α7 nAChR subtype (1.27 ± 0.04, $n = 3$). Surprisingly, moderate inhibition of the α9α10 nAChR subtype was observed (0.59 ± 01%, $n = 3$) (Fig. 4*A*). We next tested higher concentrations of [F9A]AuIB at α7 and α4β4 nAChR subtypes. Unlike the α3β4

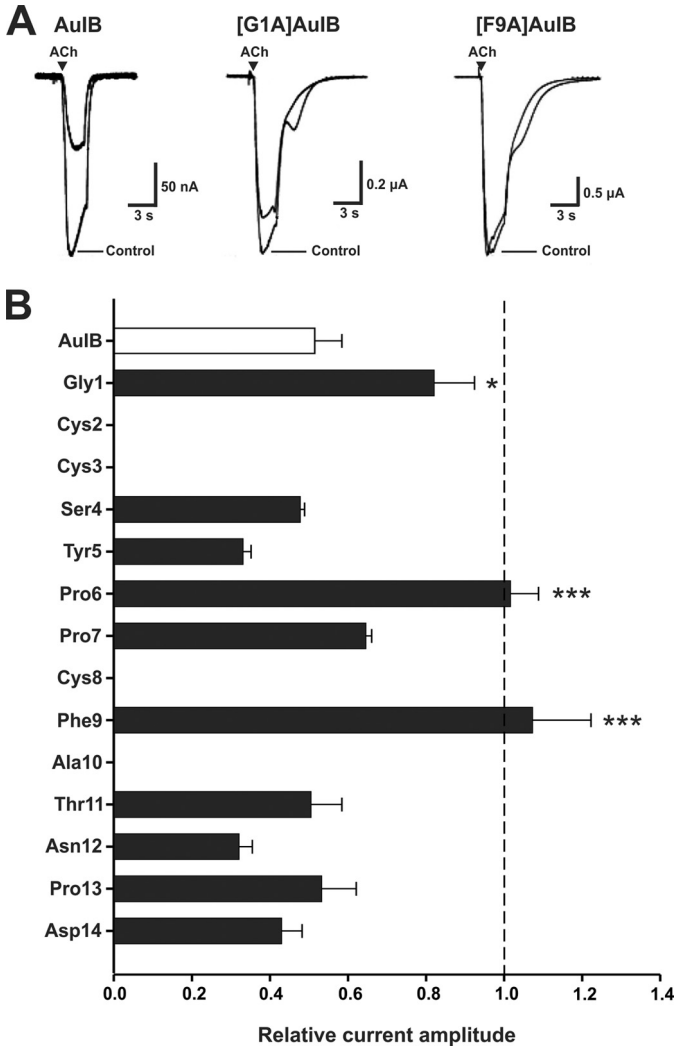

FIGURE 2. **Alanine-scanning mutagenesis of AuIB.** *A*, representative current traces showing inhibition of α3β4 ACh-evoked currents by native and alanine-substituted AuIB analogues (3 μM). *B*, *bar graph* showing ACh-evoked current inhibition of α3β4 nAChR by alanine-substituted AuIB analogues (*filled bars*) compared with native AuIB (*open bar*). All peptides used in this experiment were tested at 3 μM. Data represent the means ± S.E., $n = 3–6$. * indicates $p < 0.05$; *** indicates $p < 0.001$ for relative reduction of current inhibition *versus* native AuIB.

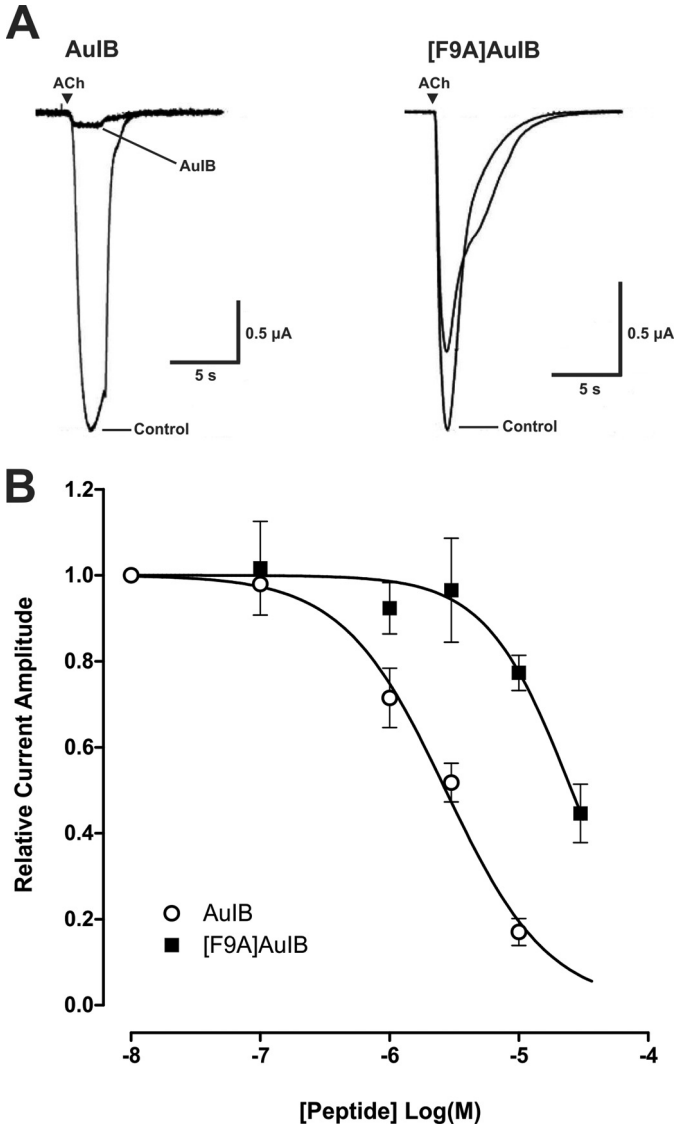

FIGURE 3. **The [F9A]AuIB analog exhibits substantially reduced activity at α3β4 nAChR.** *A*, representative ACh-evoked current traces mediated by α3β4 nAChRs in the absence and presence of native AuIB and [F9A]AuIB (10 μM). Note the substantially reduced inhibition by the [F9A]AuIB. *B*, concentration-response curves for inhibition of ACh-evoked currents by native AuIB (*open circles*) and analog [F9A]AuIB (*filled squares*). Data represent the means ± S.E., $n = 3–6$. Note that [F9A]AuIB does not attenuate inhibition but shifts the curve rightward.

nAChR subtype, where higher concentrations of [F9A]AuIB significantly inhibited ACh-evoked currents (Fig. 4*B*, see also Fig. 3*B*), no significant change in relative current amplitude was observed at α4β4 nAChRs by 10 μM (0.88 ± 0.07, $n = 4$) or 30 μM (0.85 ± 0.1, $n = 4$) of [F9A]AuIB. Similarly, at α7 nAChRs neither 10 μM (1.01 ± 0.15, $n = 4$) nor 30 μM (0.83 ± 0.35, $n = 6$) [F9A]AuIB produced any potentiation or inhibition of ACh-evoked current amplitude (Fig. 4*B*).

Homology Modeling and MD Simulations Suggest Loss of Interactions between AuIB and Key Receptor Residues When Ala Is Substituted for Phe-9—Having established that position 9 Phe in AuIB is crucial for the peptide inhibiting α3β4, we used atomistic simulations of native AuIB and the [F9A]AuIB mutant bound to α3β4 to provide molecular-level explanations of why the mutation so markedly reduces inhibition. In particular, whereas experimental alanine scanning mutagenesis on AuIB identified peptide residues crucial for its efficacy, homology modeling and MD simulations identified receptor residues that might play important roles in AuIB inhibition of α3β4 nAChR. Representative homology models of AuIB-bound α3β4 are shown in Fig. 5, *A* and *B*.

To elucidate which receptor residues probably need contact with the peptide for inhibition to occur, we first calculated the average number of interatomic contacts between native AuIB or [F9A]AuIB and each receptor ectodomain residue. We then subtracted the number of contacts between each receptor residue and [F9A]AuIB from the number of contacts between each receptor residue and native AuIB. This measured the loss (or gain) of peptide contacts at each receptor residue caused by the mutation at AuIB position 9. Receptor residues with a negative contact difference might be important for AuIB inhibition. Fig.

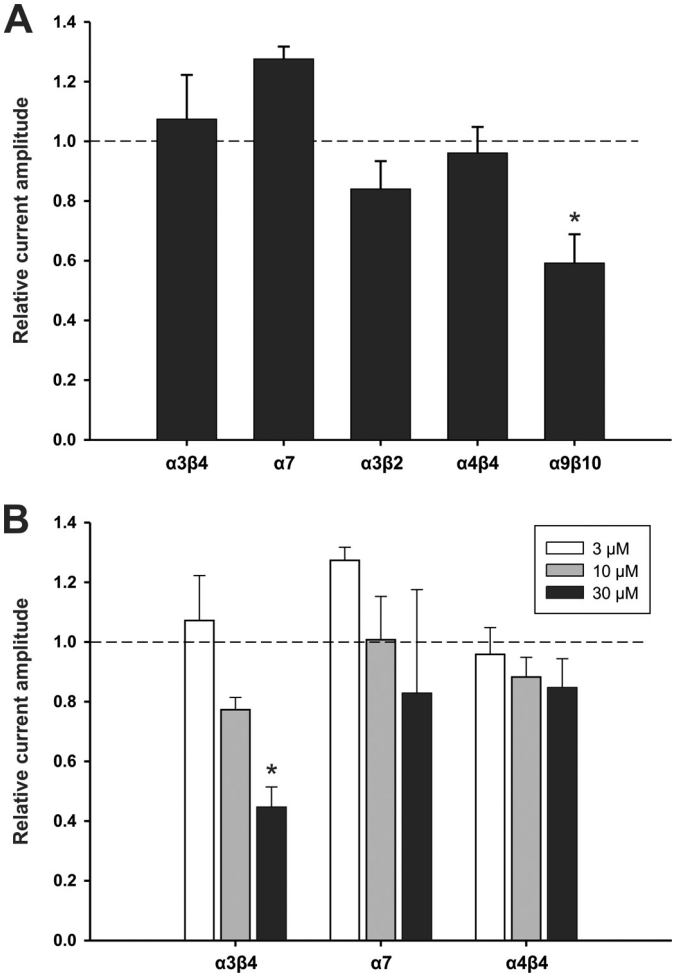

FIGURE 4. **nAChR subtype selectivity profile of [F9A]AuIB.** *A, bar graph* showing relative ACh-evoked current amplitude in the presence of 3 μM [F9A]AuIB tested at different nAChR subtypes. *B*, comparison of effects of three different [F9A]AuIB concentrations (3, 10, and 30 μM) on ACh-evoked current amplitude at rα3β4, hα7, and rα4β4 nAChR subtypes. Data represent the means ± S.E., $n = 3–6$. * indicates $p < 0.05$ for relative change of current inhibition at various nAChR subtypes *versus* α3β4 nAChRs (*A*) and for relative change of current inhibition at 10 and 30 μM compared with 3 μM peptide concentration (*B*).

5*C* shows the α3β4 receptor residues and mutation-induced changes in terms of the number of contacts with the peptide.

At the α3(+) face, loss of peptide contact at several residues (*e.g.* Tyr-93, Cys-192, and Cys-193) is offset by increased contact at others (*e.g.* Ile-188, Tyr-190, Glu-195, Tyr-197, Gln-198, and Asp-199). Therefore, on average, peptide contact at the (+) face slightly increased. In contrast, at the β4(−) face, the F9A mutation caused widespread loss of contact across many residues (with notable exceptions at Arg-115). Therefore, removing the bulky phenyl side chain at position 9 makes AuIB detach from the β4(−) face. This slightly increased the peptide's number of interatomic contacts at the opposing α3(+) face.

Based on this analysis, we propose several specific receptor residues that are especially important for AuIB inhibition of α3β4. First, because we demonstrated that the F9A mutation substantially reduces AuIB inhibitory efficacy, we examined the receptor residues that bind Phe-9, because these are probably crucial for AuIB inhibition of α3β4. The homology model and MD simulation trajectory of wild-type AuIB/α3β4 suggested that Phe-9 makes contact exclusively at the β4(−) face, with its phenyl ring sandwiched between the Trp-59 indole ring and hydrocarbon segment of the Lys-61 side chain (Fig. 6*B*). As expected, both of these residues lose contact with the peptide when position 9 of AuIB is substituted (Fig. 5*C*).

The geometry of contacts between AuIB-Phe-9 with β4-Trp-59 and β4-Lys-61 suggests that cation-π and π-π interactions may be important in AuIB inhibition of α3β4. However, we caution that the CHARMM27 force field does not explicitly account for interactions involving π electrons and acknowledge that methods which explicitly model cation-π interactions are needed to produce quantitatively accurate geometries involving charged and aromatic side chains. Nonetheless, the force field we used partially mimicked cation-π interactions and predicted Lys-Phe and Phe-Trp interaction geometries that are qualitatively in agreement with similar interactions observed in the PDB. In particular, our simulation suggests that contacts are made between β4-Lys-61 and the AuIB-Phe-9 phenyl ring primarily through the methylene carbons adjacent to the amine. In the PDB, Lys is known to engage with π systems more commonly via carbon (38, 39). Furthermore, our simulation suggests an offset-stacked interaction between β4-Trp-59 and AuIB-Phe-9. This geometry was identified as a common structural motif in Trp-Phe interactions in the PDB (40).

In addition, at the α3(+) face, there is modest but statistically significant loss of contact between AuIB and both C-loop cysteines when position 9 of AuIB is substituted (Fig. 5*C*). This is due to reduced contact between the AuIB-Cys2/8 cysteines and α3-Cys-192/193. A snapshot from the MD trajectory of the native AuIB (Fig. 6*C*) illustrates close contact between the Cys-2–8 sulfurs of the peptide and the Cys-192/193 sulfurs of α3. In contrast, a similar snapshot for the [F9A]AuIB trajectory (Fig. 6*D*) illustrates loss of close contacts between the peptide and receptor disulfides. This result is especially intriguing, given that direct contact between peptide and C-loop cysteines is proposed to be essential for the peptide competitive antagonism of nAChRs, based on results from dicarba-conotoxin variants (41). Fewer close interatomic contacts between AuIB and α3 C-loop cysteines, indirectly caused by substituting Ala for Phe at position 9 (which lies on the opposite side of the peptide), may contribute to loss of inhibitory efficacy of this mutant. Therefore, we propose that Phe-9 has two roles in the AuIB inhibition of α3β4: 1) direct contact with β4-Trp-59 and Lys-61 and 2) indirect facilitation of close contact between AuIB Cys-2/8 and α3-Cys-192/193.

Site-directed Mutagenesis of the β4 nAChR Subunit Verifies the Putative Binding Pocket on the β4 as the Site of Interaction between AuIB Phe-9 and α3β4 nAChRs—Homology modeling and MD simulations indicated that the two residues on the (−) (complementary) side of the β4 subunit sandwich Phe-9 of AuIB. We further focused on the contribution of these residues to AuIB activity at the α3β4 nAChR. We used site-directed mutagenesis of the β4 nAChR subunit to verify what role β4-Trp-59 and β4-Lys-61 have in forming a binding pocket for AuIB Phe-9. When β4-Trp-59 and β4-Lys-61 were both mutated to alanines ([W59A]+[K61A]β4), the mutant α3β4 receptor produced much smaller ACh-evoked peak current amplitudes than those of wild-type nAChR. The same effect

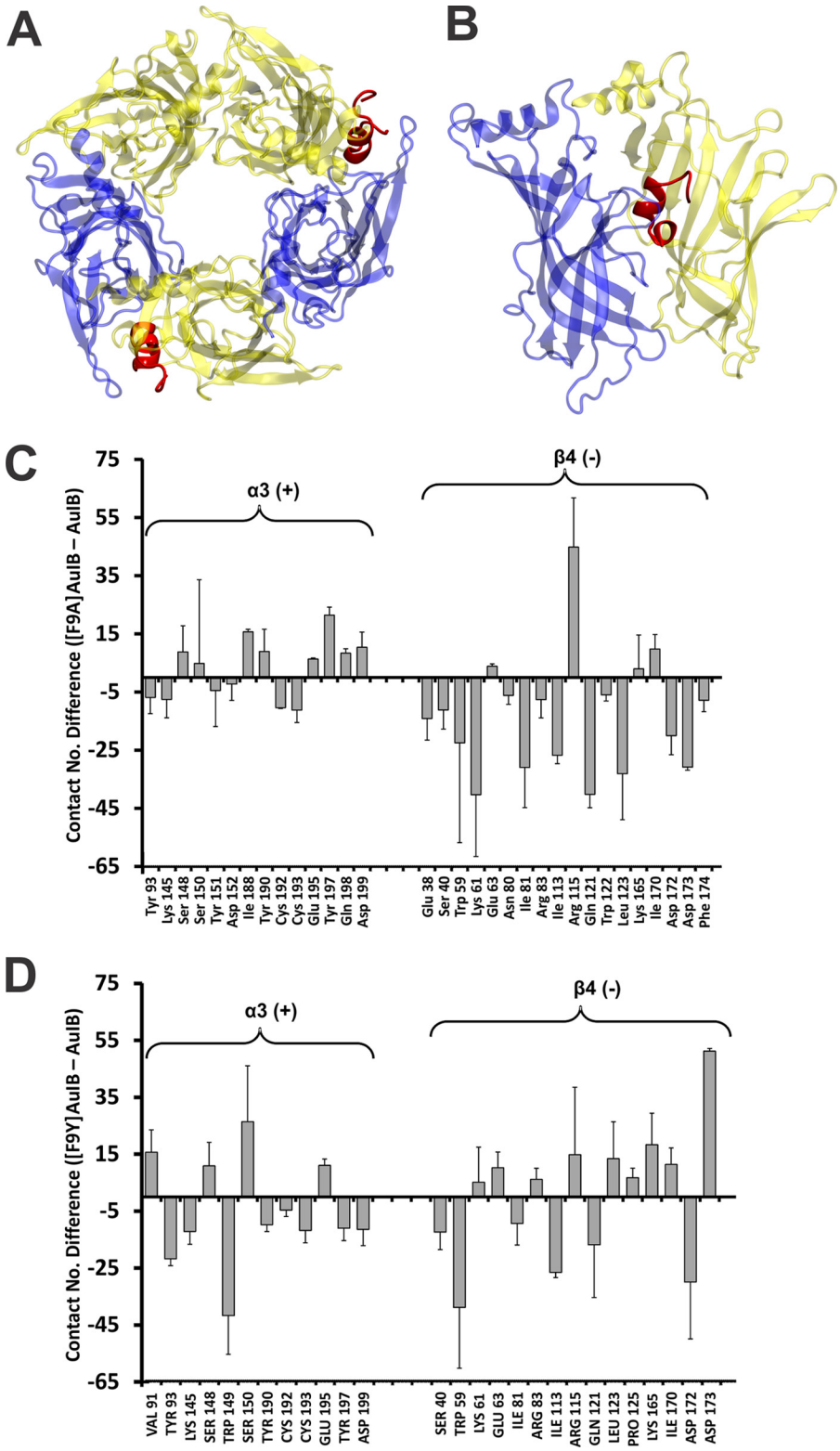

FIGURE 5. **MD simulation suggests that substituting Ala for Phe at position 9 of AulB reduces interaction between AulB and the β4 nAChR subunit.** A model shows α3β4 nAChR in the $(\alpha3)_2(\beta4)_3$ stoichiometry in top view (*A*) and its α3(+)/β4(−) interface in side view (*B*). AulB binding to the receptor is shown in *red*. *C*, contact difference *bar graph* representing quantification of results from homology modeling and MD calculations (20 ns). Shown is the number of interatomic contacts in the α3(+)/β4(−) subunit interface (<0.45 nm) between each receptor residue and the bound peptide lost (negative *y* axis values) or gained (positive *y* axis values) as a result of substituting Ala-9 for Phe-9. Note that the effect at the β4(−) side is a loss of interaction between [F9A]AulB and the β4 subunit. *D*, a contact difference *bar graph* for [F9Y]AulB indicates mutation to Tyr results in substantial loss of contacts between the peptide and several aromatic cage residues at the α3 (Tyr-93, Trp-149, Tyr-197) and β4 (Trp-59) subunits. Furthermore, the number of contacts with the α3-Cys192/193 sulfurs is reduced.

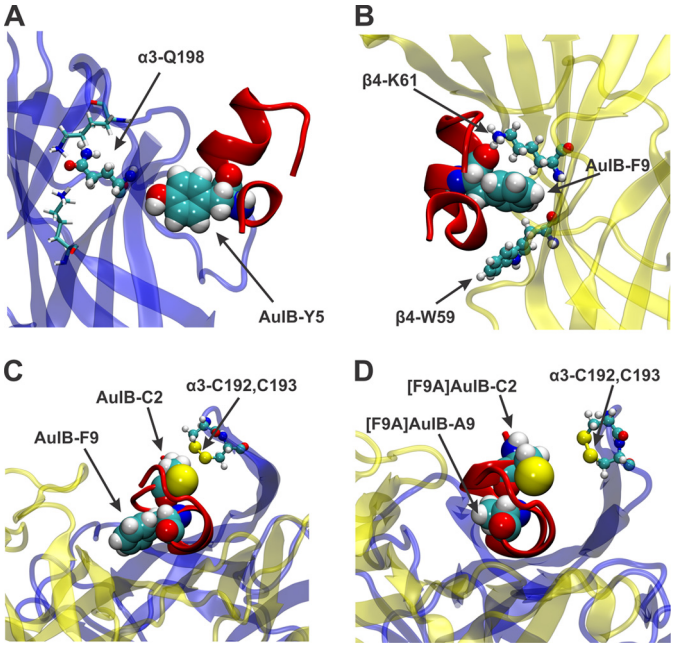

FIGURE 6. **Homology modeling and MD simulation of AuIB·α3β4 binding.** *A*, main interacting residues between AuIB and α3 subunit. Receptor backbone is in *transparent blue ribbon* form, with receptor residues of interest in Corey-Pauling-Koltun representation and indicated with *arrows*. Peptide backbone is in *opaque red ribbon* form, with residues of interest shown as van der Waals spheres and indicated with *arrows*. *B*, main interacting residues between AuIB and β4 subunit. Receptor backbone is in *transparent yellow ribbon* form. At the α3(+) β4(−) interface, the only "unique α3" residue making direct contact with AuIB is Gln-198. However, this occurs via backbone only. On the β4 subunit, Phe-9 of AuIB is stabilized by Lys-61 and Trp-59 of the receptor. Phe-9 substitution to alanine results in loss of interactions with both these residues. Trp-59 is common to all neuronal nAChRs and so does not determine AuIB selectivity. Lys-61 is unique to the β4 subunit, so determines AuIB selectivity for α3β4. *C*, snapshot illustrating close contact between AuIB-Cys2 (van der Waals spheres) and α3(+)-Cys-192 and -Cys-193 (Corey-Pauling-Koltun representation). *D*, snapshot illustrating loss of close contact between [F9A]AuIB-Cys2 and α3(+)-Cys192 and -193, which might be partly responsible for loss of inhibitory activity of [F9A]AuIB and [F9Y]AuIB.

was present when β4-Trp-59 was mutated alone ([W59A]β4). Therefore, we used a high agonist concentration (2.5 mM ACh) to evoke currents in all groups to create a meaningful comparison. The high agonist concentration should not interfere with AuIB inhibition, because AuIB inhibits the α3β4 nAChR noncompetitively irrespective of ACh concentration (14). We assessed the effect of β4 mutations using a high concentration of native AuIB (10 μM), which efficiently inhibits wild-type α3β4 nAChRs (14).

The [W59A]+[K61A]β4 mutation almost completely abolished inhibition by native AuIB (0.89 ± 0.08, $n = 6$) compared with wild-type β4 (0.15 ± 0.07, $n = 5$) (Fig. 7, *A* and *B*). The same abolishing effect was observed with the [W59A]β4 mutant in which only β4-Trp-59 was changed to Ala (0.89 ± 0.05, $n = 3$). However, slightly more inhibitory activity remained with the [K61A]β4 mutation (0.66 ± 0.03, $n = 3$) (Fig. 7, *A* and *B*). This suggests that β4-Trp-59 and β4-Lys-61 help form the pocket for interaction between the receptor and Phe-9 of AuIB. However, in contrast with the auxiliary role of β4-Lys-61, interaction between the two aromatic residues of the peptide and receptor (Phe-9-AuIB·β4-Trp-59) appears indispensable for mediating AuIB inhibitory effect. We also tried to make a control mutation of a tryptophan further down the sequence from the ACh binding site ([W64A]β4), but no ACh-induced current was elicited at the mutated receptor.

Our model suggested that Tyr-5 of AuIB probably interacts with the backbone of Gln-198 of the α3 subunit (Fig. 6*A*). A mutation of α3-Gln-198 to alanine ([Q198A]α3) had only a minor, but significant, effect on currents evoked by ACh (50 μM) and inhibited by AuIB (10 μM) (0.25 ± 0.02, $n = 5$, $p = 0.032$ for [Q198A] mutant; 0.17 ± 0.02, $n = 4$ for native AuIB). However, mutation of its putative partner, Tyr-5 of AuIB ([Y5A]AuIB), did not reduce wild-type α3β4 nAChR inhibition at 3 μM (0.33 ± 0.02, $n = 5$) (see Fig. 2*B*). Therefore, α3-Gln-198 interaction with AuIB-Tyr-5 is unlikely to determine AuIB activity.

How Side Chain Size and Hydrophobicity at Position 9 of AuIB Affect Inhibition at the α3β4 nAChR—Given the critical interaction between AuIB-Phe-9 and β4-Trp-59 and the proposed importance of cation-π and π-π interactions for the inhibitory activity of AuIB, we assessed how side chain size, aromaticity, and hydrophobicity of the amino acid residue at position 9 in the AuIB sequence affect nAChR inhibition. In particular, we sought to find position 9 substituents that may better fit the Trp-59–Lys-61 pocket on the β4 nAChR subunit than Phe. We probed the inhibitory action of AuIB analogues substituted at position 9 by large aromatic (Tyr, Trp, 3-(2-naphthyl)-L-alanine (NAL)) and small (Gly) side chains on wild-type α3β4 nAChRs. CD analysis confirmed that the globular peptide structure was retained in all of these analogues ([F9G]AuIB, [F9Y]AuIB, [F9W]AuIB, [F9NAL]AuIB) (Fig. 8*A*). Substituting Phe-9 to glycine ([F9G]AuIB, 10 μM) dramatically reduced inhibition (0.90 ± 0.04, $n = 3$; $p < 0.001$) compared with native AuIB (0.047 ± 0.01, $n = 6$) (Fig. 8*B*). This is consistent with our proposed model in which AuIB interaction with the binding pocket on the β4 subunit is crucial. This interaction is presumably absent when Phe-9 is replaced by the side chain-free Gly.

Phe-9 mutation to the slightly larger and less hydrophobic Tyr ([F9Y]) significantly reduced α3β4 nAChR inhibition (0.42 ± 0.07, $n = 3$; $p < 0.001$) (Fig. 8*B*) compared with native AuIB. Homology modeling and MD simulation of the [F9Y]AuIB·α3β4 interaction suggest that mutation to Tyr results in substantial loss of contacts between the peptide and several aromatic cage residues at the α3 (Tyr-93, Trp-149, Tyr-197) and β4 (Trp-59) subunits, as shown by contact difference plot (Fig. 5*D*) The latter residue is of special interest given its known importance for AuIB inhibition (discussed above). Inspection of the structural model indicates that the aromatic ring of Tyr-9 in [F9Y]AuIB directly contacts the hydrocarbon segment of β4-Lys-61. But unlike the Phe-9 of native AuIB (Fig. 6*B*), the Tyr-9 side chain does not contact Trp-59 β4. Furthermore, mutation to Tyr results in loss of contact with the α3-Cys-192/193 sulfurs (Fig. 5*D*). Together with the electrophysiology data, our model of [F9Y]AuIB·α3β4 interaction further supports our hypothesis that position 9 contact with the β4-Tyr-59 and α3 disulfide structural motif is essential for AuIB activity against α3β4.

Another AuIB analog in which Trp was substituted for Phe-9 (F9W) substantially reduced inhibition (0.80 ± 0.07, $n = 3$; $p <$

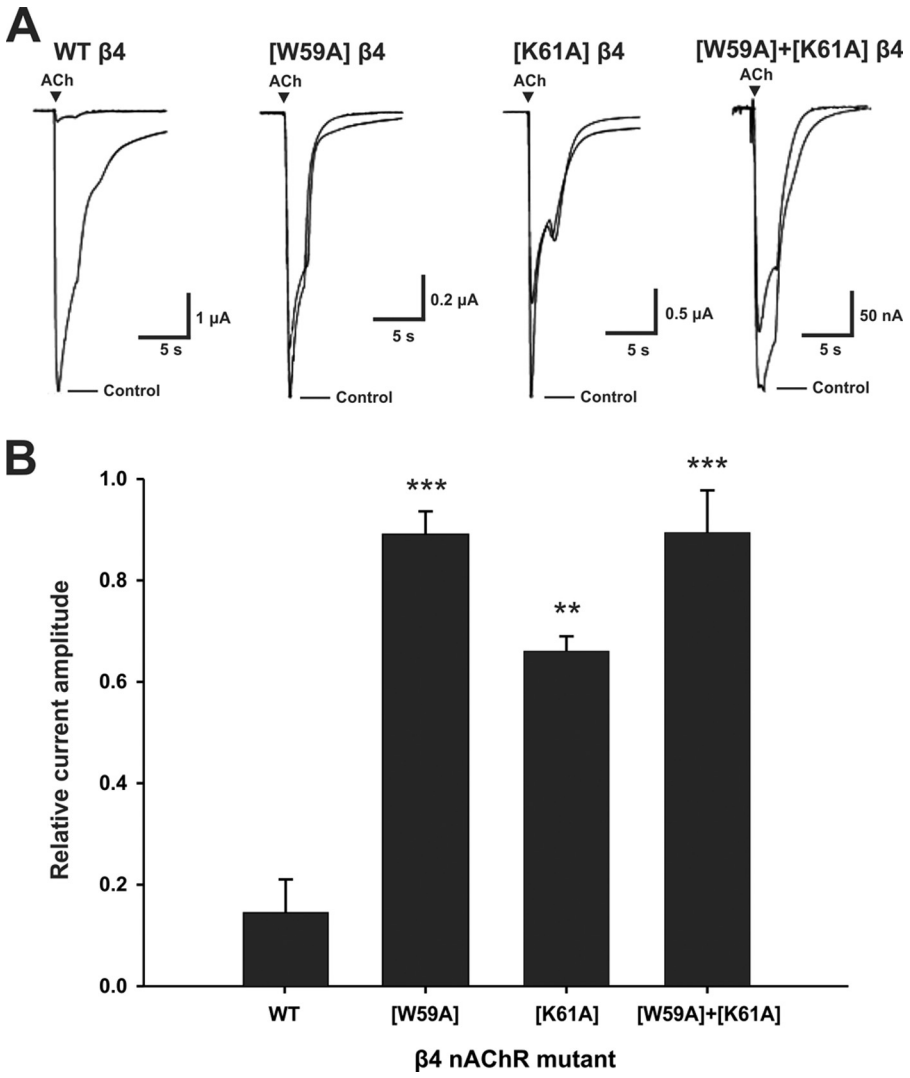

FIGURE 7. **The effects of point mutations in the β4 nAChR subunit on AuIB inhibition.** *A*, representative ACh-evoked currents showing native AuIB (10 μM) inhibition of α3β4 nAChRs compared with the β4 subunit double mutant (W59A + K61A) and two single point mutants of β4, W59A and K61A. *B*, *bar graph* showing quantification of AuIB (10 μM) inhibition at the β4 nAChR subunit mutants and wild-type α3β4 nAChR. AuIB inhibition is abolished in [W59A]β4 and the [W59A]+[K61A]β4 double mutant, confirming these residues have a key role in AuIB binding. Note the intermediate effect of K61A mutation, suggesting it has an auxiliary role in forming the binding pocket for the hydrophobic interaction with Trp-59, which is key for inhibition. Note that only high ACh concentration elicited measurable currents in the W59A+K61A mutant. Therefore, 2.5 mM ACh was used as an agonist to compare inhibition in the mutants and wild-type receptors. Data represent the means ± S.E., $n = 3–6$. ** indicates $p < 0.005$; *** indicates $p < 0.001$ for relative reduction of current inhibition *versus* wild-type α3β4 nAChRs.

0.001) presumably due to steric clashes. Indeed, automated blind docking of [F9W]AuIB to α3β4 using Autodock (42) with all peptide side chain torsions free to rotate showed that none of the docking solutions involved binding of analog [F9W]AuIB to the canonical C-loop pocket. In contrast, docking of both native and [F9Y]AuIB predicted binding conformations very close to that of the double mutant PnIA-AChBP co-crystal structure (2BR8) (data not shown). An analog with an even larger unnatural amino acid, NAL, to substitute Phe-9 ([F9NAL]AuIB) also showed dramatically reduced inhibition (0.82 ± 0.07, $n = 3$; $p < 0.001$) (Fig. 8*B*). The NAL was attached to the 2-position of the Ala residue. Unlike the Trp residue, which has an *N*-heterocyclic five ring, NAL has a homocarbocyclic six ring.

Together, these results demonstrate that side chain size, aromaticity, and hydrophobicity at position 9 of AuIB are important for interaction between the peptide and β4 subunit of the α3β4 pentamer. In contrast with the above mentioned analogues with substitutions at position 9, inhibition in a control AuIB analog with a histidine substitution at position 12 (N12H) was not significantly impaired (0.069 ± 0.003, $n = 3$) (Fig. 8*B*).

DISCUSSION

Using alanine scanning mutagenesis, we identified three residues in the AuIB sequence (Gly-1, Pro-6, and Phe-9) that affect inhibition of α3β4 nAChRs. The Gly to Ala substitution only moderately reduced inhibition. Homology modeling of the AuIB·α3β4 complex suggests that the N terminus NH_3^+ of AuIB forms a salt bridge with the β4-Asp-172 side chain. The G1A mutation introduces a non-polar CH_3 side chain that may weaken the favorable interaction between the peptide N ter-

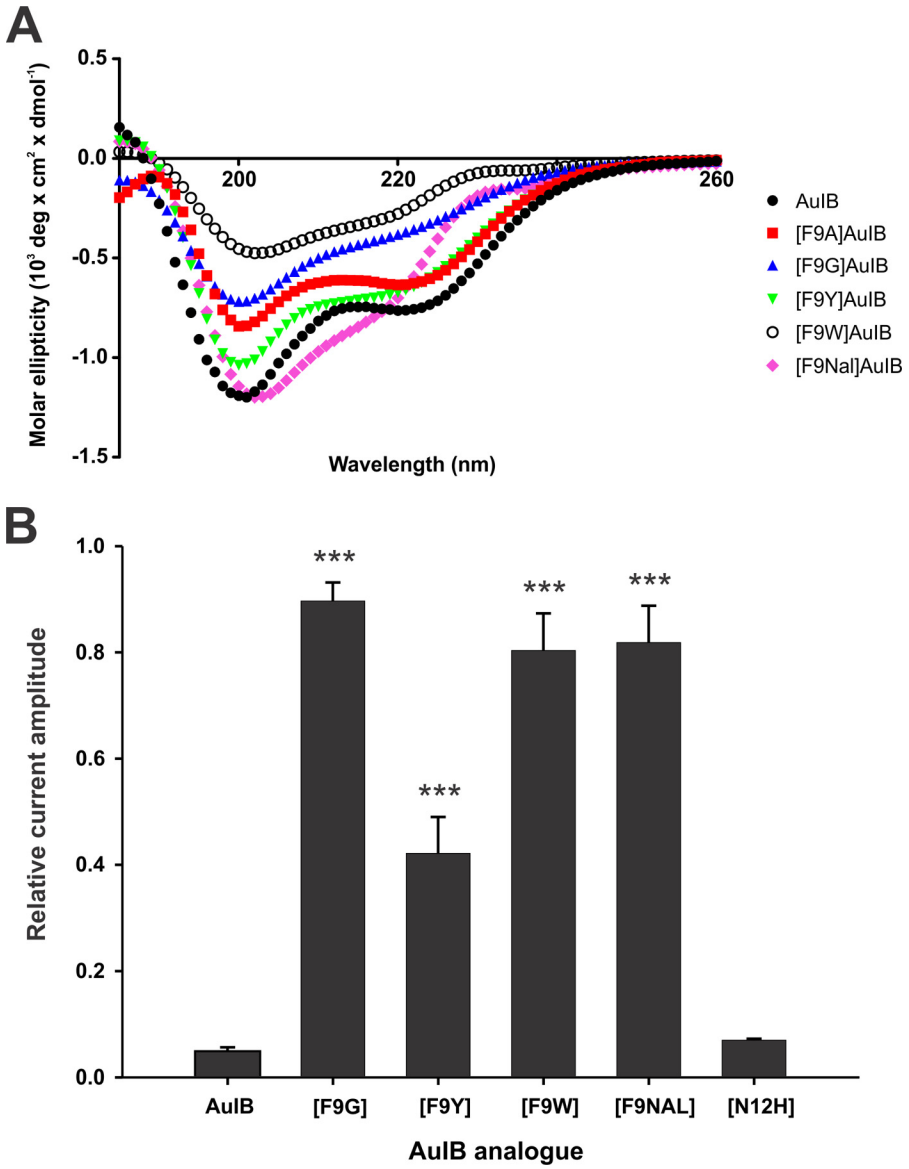

FIGURE 8. **The effects of various substitutions at position 9 of AuIB on its inhibition of the α3β4 nAChR subtype.** *A*, CD spectra of AuIB analogues in which Phe-9 was substituted by various other residues. These spectra were similar to the spectrum of native globular AuIB, confirming that all of these analogues retained their structure. *B*, *bar graph* showing inhibition of α3β4 nAChR ACh-evoked current amplitude by native AuIB and its F9-substituted analogues (10 μM). Note that inhibition is abolished if the position 9 residue is too small or too large. Still present, but reduced inhibition by the Tyr analog suggests that hydrophobic interaction with the binding pocket at the β4 subunit is reduced because of steric hindrance. A random control mutation at position 12 of AuIB ([N12H]AuIB) does not attenuate maximal inhibition by AuIB. Data represent the means ± S.E., $n = 3–6$. *** indicates $p < 0.001$ for relative reduction of current inhibition *versus* native AuIB.

minus and β4-Asp-172 side chain. Additionally, in a recent study investigating N-terminal post-translational modification of α-conotoxin MI, truncation of the N-terminal residue decreased the affinity for the muscle-type nAChR, a direct pharmacological effect indicating the N-terminal residues are important for bioactivity (43). α-Conotoxin LsIA has also shown reduced potency at α7 and α3β2 nAChRs when N-terminally truncated (44), which corroborates the potential importance of the N-terminal amino acid in α-conotoxin potency and selectivity.

The other two substitutions, P6A and F9A, caused an even greater decrease in peptide activity on α3β4 nAChR than G1A. Our NMR and CD data revealed that the [P6A]AuIB analog structure is disrupted, but that of [F9A]AuIB is not. This is not surprising considering the structural effect Pro has on protein structures in general and α-conotoxin structures in particular (34). Therefore, we reasoned that the ability of Phe-9, but not Pro-6, to reduce inhibition is due to Phe-9 specifically interacting with the α3β4 nAChR. We found that the number of mutations that reduce AuIB inhibition of the α3β4 nAChR is small compared with other α-conotoxins. For instance, alanine substitutions of almost all intercysteine residues in another α-conotoxin, Vc1.1, affected α9α10 nAChR inhibition (35). We also found no alanine mutants that inhibited the α3β4 nAChR significantly more than native AuIB.

As well as substantially reducing α3β4 inhibition, [F9A]AuIB selectivity for nAChR subtypes also shifted. This indicates that Phe-9 has a role in the peptide specific interaction with the

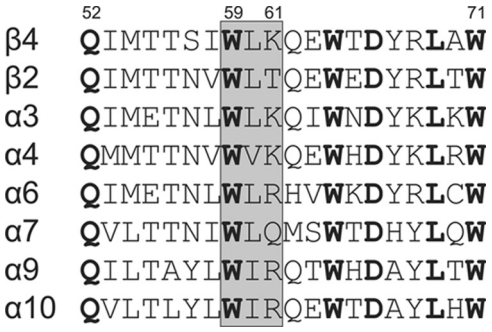

FIGURE 9. **Protein sequence alignment of nAChR subunits.** Sequence alignments showing the (−)(complementary) side of the main neuronal nAChR subunits centered around loop D and its conserved tryptophan residue TrpD, the main β4 subunit residue that interacts with Phe-9 of AuIB (β4-Trp-59). Absolutely conserved residues in the sequences are emphasized in *bold*. *Boxed residues* are homologous to the WLK binding pocket on β4(−) subunit. Residue numbering according to the β4 subunit sequence is shown. Note the ubiquitous conservation of tryptophan.

α3β4 nAChR and is needed to maintain selectivity for this particular subtype. Our docking simulation and MD calculations showed that the (−) side of the β4 subunit is the site where AuIB makes the most intermolecular contacts. Modeling also suggested that Phe-9 is sandwiched by Trp-59 and Lys-61, which may form a binding pocket on the β4 subunit. This model's validity was corroborated by mutational analysis of the β4 subunit and position 9 of AuIB.

The Role of the β4 nAChR Loop D and Its Conserved Tryptophan in Binding to AuIB and the Pharmacology of Various Ligands—Analysis of the β4 sequence (see also Fig. 9) indicates that the AuIB binding pocket partially overlaps with the ACh binding site. Residues 59–61 are situated on the β2 strand of the β4 subunit and form the main functional part of loop D on the complementary ACh-binding site component. The tryptophan of loop D (TrpD; Trp-59 in β4 numbering) is highly conserved across different nAChR subunits and AChBPs and helps form the aromatic box/cage of hydrophobic residues essential for ACh binding and nAChR activation (45, 46). The residue in position +2 relative to TrpD (Lys-61 in β4 numbering) is also an important part of the ACh binding site (*e.g.* it corresponds with Gln-57 in the α7 subunit).

Studies involving receptor mutations and co-crystallization with AChBPs have shown that α-conotoxins bind in the extracellular part of nAChR subunit interface close to the ligand binding site (47, 48). Usually α-conotoxins do not rely on a single critical residue/contact, and their binding determinants can be found on both principal and complementary sides. For instance, ImI has been proposed to bind to AChBP via a "network of interactions" (49). Similar findings were obtained in an earlier ImI-AChBP co-crystallization study (47) and using docking simulations for ImI, GIC, MII, PnIA, and GID (50–52). A study measuring ImI binding to mutated α7 nAChRs reported a single dominant interaction between Arg-7 of ImI and Tyr-195 of α7 as well as multiple weak interactions between several other residues (53).

Many non-peptide ligands bind in the loop D region (54–57), and in some cases, the residues homologous to β4-Lys-61 were also suggested to be important. For example, differences in sensitivity between α3β4 and α3β2 to receptor antagonists dihydro-β-erythroidine and bungarotoxin and to agonists ACh and nicotine were explained by the same difference in the sequence (Lys-61 at β4; Thr-59 in β2 numbering) (55, 56). A residue in this position underlies a difference between insect and vertebrate nAChRs in sensitivity to neonicotinoid insecticides (57). A difference in two residues preceding TrpD accounts for a remarkable difference in human *versus* rat α3β4 nAChR sensitivity to the agonist 5-(trifluoromethyl)-6-(1-methyl-azepan-4-yl)methyl-1*H*-quinolin-2-one (TMAQ) (54).

Using α3β2 receptor chimeras, determinants for MII conotoxin specificity were found on α and β subunits (58). Interestingly, one of the determinants was mapped to loop D of the β2 subunit and identified as Thr-59 (homologous to β4-Lys-61). Therefore, the Lys to Thr substitution in the β2 subunit was one factor that defined β2/β4 selectivity for MII. BuIA conotoxin has a different wash-off rate for α3β2 than α3β4 nAChRs. The same difference in the sequence (Lys/Thr-59) in β4 and β2 was also a determinant for the different wash-off rates for the various nAChR subtypes (59).

Consistent with the studies mentioned above, our modeling and experimental data show that the β4 single-point mutation [K61A]β4 only reduces AuIB inhibition, but [W59A]β4 (TrpD) completely abolishes it. Therefore, TrpD is essential for AuIB to inhibit α3β4 nAChRs. TrpD involvement in nAChR pharmacology is well documented. Mutations of TrpD in AChBP have been shown to affect its conformation as well as alter its potency, desensitization, efficacy, and selectivity for various ligands (60–64). However, its effects depend on the subunit and ligand in question and are more ambiguous than mutations of the principal subunit's aromatic residues. For instance, the effects of the TrpD mutation on ACh affinity for muscle nAChRs differed between δ and γ subunits (20,000 *versus* 7,000-fold reduction) (61). TrpD mutation caused opposite shifts in the potency of 4OH-GTS21 agonists in α7 and α4β2 nAChRs (62).

When expressed in *Xenopus* oocytes and tested by two-voltage clamp recordings, the [W59A]β4 mutation dramatically reduced the ACh-induced current without altering its kinetics. To induce measurable currents, we had to use the saturating ACh concentration of 2.5 mM instead of 50 μM. In a previous study we showed that high ACh concentration has practically no effect on AuIB inhibition of α3β4, as this inhibition is non-competitive (14).

There are examples where the binding/action of pharmacological agents is critically dependent on interaction with TrpD. Apolipoprotein E inhibits α7 nAChRs via hydrophobic interactions with α7 TrpD (Trp55 in α7 numbering) (64). Varenicline, a smoking cessation drug, has been shown to interact with β2-TrpD in the α4β2 nAChR. TrpD substitution to Ala converted varenicline from a partial to full agonist and abolished varenicline-induced desensitization at high concentrations (63).

Nature of AuIB-Phe-9·β4-Trp-59 Interaction and Its Implications for AuIB Pharmacology—The sequence alignment of several nAChR subunits (Fig. 9) centered at the AuIB binding pocket shows that only TrpD (Trp-59 in β4 numbering) is absolutely conserved across the different subunits. However, substitutions in the WLK pocket are often homologous. For example,

instead of β4-Lys at the TrpD +2 position, α9 and α10 subunits have a similar positively charged Arg. There is a single different residue, Thr instead of Lys, between β2 and β4, and this can cause differences in pharmacology. It is unlikely that Lys/Thr substitution underlies AuIB selectivity for the α3β4 subtype, as the [K61A]β4 mutation only reduces inhibition, and AuIB is not active at the α9α10 subtype when Lys is changed to an essentially homologous Arg. Interestingly, loop D of the α3 subunit has the same WLK pocket as the β4 subunit.

AuIB could also bind at the non-canonical binding site (+)β/(−)α, as suggested for galanthamine and cocaine binding to AChBP (65), anti-helminthic compound morantel binding to α3β2 nAChRs (66), and recently for α-conotoxin Vc1.1 binding to α9α10 nAChRs (67). However, this is unlikely because the docking model does not support binding at a non-canonical site and the [W59A]β4 mutant loses inhibition despite identical WLK pockets being available on the α3 subunit (−) side. Another possibility could be that AuIB anchoring at the WLK pocket is controlled by its interactions with the α subunit.

Our homology and MD-simulated model suggested that Tyr-5 of AuIB interacts with the α3 subunit Gln-198. However, [Q198A]α3 mutation did not affect AuIB inhibition, and mutation of its putative partner, Tyr-5-AuIB, did not reduce inhibition on the wild-type receptor. Mounting evidence suggests that differences in three-dimensional structure across subunits probably underlies distinct bond patterns for the same ligand despite the presence of identical residues, as demonstrated for nicotinic ligands (68, 69). This is certainly possible for larger molecules, such as AuIB.

There is also the question of the mechanism behind AuIB inhibition of nAChRs and how it can act non-competitively despite overlapping with the ACh-binding site. At least two larger peptides, apolipoprotein E and $A\beta_{1-42}$ amyloid, block nAChRs non-competitively as well. In addition, apolipoprotein E binds to loop D by interacting with TrpD (64, 70). AuIB may be able to act non-competitively because it can bind to α3β4 in the presence of ACh. Because TrpD may be involved in desensitizing or transducing the gating signal (54, 63, 71), AuIB may work by stabilizing the desensitized state or blocking the gating signal. Another possibility is steric hindrance to the movement of loop C, which is thought to be associated with agonist activation of nAChRs (47, 72).

What could be the nature of the AuIB-Phe-9 interaction with TrpD? It is well established that residues around ligand binding sites and those that form the aromatic box in Cys-loop family receptors often make cation-π bonds with their cognate ligands (73). The reverse situation, when aromatic moieties of ligands engage in a cation-π bond formation with positively charged residues of the receptor, is also possible (74). AuIB does not have positively charged residues so cannot make a cation-π bond with β4-Trp-59 (TrpD). A situation in which a positively charged β4-Lys-61 forms a cation-π bond with Phe-9 of AuIB is possible. However, our experiment with single-point mutations of the WLK pocket showed that removing Lys-61 does not abolish inhibition but that Trp-59 mutation does. This suggests that Trp-59 is indispensable for AuIB inhibitory effect and Lys-61 plays an auxiliary role in it.

Our experiments with second-generation AuIB mutants at position 9 demonstrated that size and hydrophobicity/aromaticity of the residue in this position are important for the peptide to inhibit α3β4 nAChRs. Although simple hydrophobic interaction of AuIB-Phe-9 and β4-Trp-59 is possible, it is more likely that Phe-9 and Trp-59 interact via π-π stacking due to the deep insertion of Phe-9 in the WLK pocket. Because removing positively charged Lys-61 reduces inhibition, it will likely interact with Phe-9 of AuIB and/or stabilize AuIB-Phe-9 interaction with β4-Trp-59. In conclusion, we identified determinants of AuIB binding/action on the α3β4 nAChR.

Acknowledgments—A. H. and D. J. A. thank the Victorian Life Sciences Computation Initiative and IBM Collaboratory for Life Sciences (Melbourne) for providing CPU hours under Resource Grant VR0009.

REFERENCES

1. Olivera, B. M., Rivier, J., Clark, C., Ramilo, C. A., Corpuz, G. P., Abogadie, F. C., Mena, E. E., Woodward, S. R., Hillyard, D. R., and Cruz, L. J. (1990) Diversity of *Conus* neuropeptides. *Science* **249,** 257–263
2. Lewis, R. J., and Garcia, M. L. (2003) Therapeutic potential of venom peptides. *Nat. Rev. Drug Discov.* **2,** 790–802
3. Terlau, H., and Olivera, B. M. (2004) *Conus* venoms. A rich source of novel ion channel-targeted peptides. *Physiol. Rev.* **84,** 41–68
4. Armishaw, C. J., and Alewood, P. F. (2005) Conotoxins as research tools and drug leads. *Curr. Protein Pept. Sci.* **6,** 221–240
5. Han, T. S., Teichert, R. W., Olivera, B. M., and Bulaj, G. (2008) *Conus* venoms. A rich source of peptide-based therapeutics. *Curr. Pharm. Des.* **14,** 2462–2479
6. Azam, L., and McIntosh, J. M. (2009) α-Conotoxins as pharmacological probes of nicotinic acetylcholine receptors. *Acta Pharmacol. Sin.* **30,** 771–783
7. Janes, R. W. (2005) α-Conotoxins as selective probes for nicotinic acetylcholine receptor subclasses. *Curr. Opin. Pharmacol.* **5,** 280–292
8. Albuquerque, E. X., Pereira, E. F., Alkondon, M., and Rogers, S. W. (2009) Mammalian nicotinic acetylcholine receptors. From structure to function. *Physiol. Rev.* **89,** 73–120
9. Tapper, A. R., McKinney, S. L., Nashmi, R., Schwarz, J., Deshpande, P., Labarca, C., Whiteaker, P., Marks, M. J., Collins, A. C., and Lester, H. A. (2004) Nicotine activation of α4* receptors. Sufficient for reward, tolerance, and sensitization. *Science* **306,** 1029–1032
10. Improgo, M. R., Scofield, M. D., Tapper, A. R., and Gardner, P. D. (2010) The nicotinic acetylcholine receptor CHRNA5/A3/B4 gene cluster. Dual role in nicotine addiction and lung cancer. *Prog. Neurobiol.* **92,** 212–226
11. Hurst, R., Rollema, H., and Bertrand, D. (2013) Nicotinic acetylcholine receptors. From basic science to therapeutics. *Pharmacol. Ther.* **137,** 22–54
12. Millar, N. S., and Gotti, C. (2009) Diversity of vertebrate nicotinic acetylcholine receptors. *Neuropharmacology* **56,** 237–246
13. Unwin, N. (2005) Refined structure of the nicotinic acetylcholine receptor at 4 Å resolution. *J. Mol. Biol.* **346,** 967–989
14. Grishin, A. A., Wang, C. I., Muttenthaler, M., Alewood, P. F., Lewis, R. J., and Adams, D. J. (2010) α-Conotoxin AuIB isomers exhibit distinct inhibitory mechanisms and differential sensitivity to stoichiometry of α3β4 nicotinic acetylcholine receptors. *J. Biol. Chem.* **285,** 22254–22263
15. Luo, S., Kulak, J. M., Cartier, G. E., Jacobsen, R. B., Yoshikami, D., Olivera, B. M., and McIntosh, J. M. (1998) α-Conotoxin AuIB selectively blocks α3β4 nicotinic acetylcholine receptors and nicotine-evoked norepinephrine release. *J. Neurosci.* **18,** 8571–8579
16. Azam, L., Dowell, C., Watkins, M., Stitzel, J. A., Olivera, B. M., and McIntosh, J. M. (2005) α-Conotoxin BuIA, a novel peptide from *Conus bullatus*, distinguishes among neuronal nicotinic acetylcholine receptors. *J. Biol. Chem.* **280,** 80–87
17. Franco, A., Kompella, S. N., Akondi, K. B., Melaun, C., Daly, N. L., Luetje,

C. W., Alewood, P. F., Craik, D. J., Adams, D. J., and Marí, F. (2012) RegIIA. An α4/7-conotoxin from the venom of *Conus regius* that potently blocks α3β4 nAChRs. *Biochem. Pharmacol.* **83,** 419–426
18. Clark, R. J., Fischer, H., Nevin, S. T., Adams, D. J., and Craik, D. J. (2006) The synthesis, structural characterization, and receptor specificity of the α-conotoxin Vc1.1. *J. Biol. Chem.* **281,** 23254–23263
19. Innocent, N., Livingstone, P. D., Hone, A., Kimura, A., Young, T., Whiteaker, P., McIntosh, J. M., and Wonnacott, S. (2008) α-Conotoxin arenatus IB[V11L,V16D] is a potent and selective antagonist at rat and human native α7 nicotinic acetylcholine receptors. *J. Pharmacol. Exp. Ther.* **327,** 529–537
20. Pereira, E. F., Alkondon, M., McIntosh, J. M., and Albuquerque, E. X. (1996) α-Conotoxin-ImI. A competitive antagonist at α-bungarotoxin-sensitive neuronal nicotinic receptors in hippocampal neurons. *J. Pharmacol. Exp. Ther.* **278,** 1472–1483
21. Dutton, J. L., Bansal, P. S., Hogg, R. C., Adams, D. J., Alewood, P. F., and Craik, D. J. (2002) A new level of conotoxin diversity, a non-native disulfide bond connectivity in α-conotoxin AuIB reduces structural definition but increases biological activity. *J. Biol. Chem.* **277,** 48849–48857
22. Sandall, D. W., Satkunanathan, N., Keays, D. A., Polidano, M. A., Liping, X., Pham, V., Down, J. G., Khalil, Z., Livett, B. G., and Gayler, K. R. (2003) A novel α-conotoxin identified by gene sequencing is active in suppressing the vascular response to selective stimulation of sensory nerves *in vivo*. *Biochemistry* **42,** 6904–6911
23. Satkunanathan, N., Livett, B., Gayler, K., Sandall, D., Down, J., and Khalil, Z. (2005) α-Conotoxin Vc1.1 alleviates neuropathic pain and accelerates functional recovery of injured neurones. *Brain Res.* **1059,** 149–158
24. Klimis, H., Adams, D. J., Callaghan, B., Nevin, S., Alewood, P. F., Vaughan, C. W., Mozar, C. A., and Christie, M. J. (2011) A novel mechanism of inhibition of high-voltage activated calcium channels by α-conotoxins contributes to relief of nerve injury-induced neuropathic pain. *Pain* **152,** 259–266
25. Callaghan, B., Haythornthwaite, A., Berecki, G., Clark, R. J., Craik, D. J., and Adams, D. J. (2008) Analgesic α-conotoxins Vc1.1 and RgIA inhibit N-type calcium channels in rat sensory neurons via $GABA_B$ receptor activation. *J. Neurosci.* **28,** 10943–10951
26. Callaghan, B., and Adams, D. J. (2010) Analgesic α-conotoxins Vc1.1 and RgIA inhibit N-type calcium channels in sensory neurons of α9 nicotinic receptor knockout mice. *Channels* **4,** 51–54
27. Cuny, H., de Faoite, A., Huynh, T. G., Yasuda, T., Berecki, G., and Adams, D. J. (2012) γ-Aminobutyric acid type B ($GABA_B$) receptor expression is needed for inhibition of N-type (Cav2.2) calcium channels by analgesic α-conotoxins. *J. Biol. Chem.* **287,** 23948–23957
28. Adams, D. J., and Berecki, G. (2013) Mechanisms of conotoxin inhibition of N-type (Cav2.2) calcium channels. *Biochim. Biophys. Acta* **1828,** 1619–1628
29. Cuny, H., Grishin, A. A., Hung, A., R. J., C., Akondi, K., Brust, A., Alewood, P. F., Craik, D. J., and Adams, D. J. (2012) Identifying key amino acid residues for α-conotoxin AuIB inhibition of α3β4 nicotinic acetylcholine receptors. *Proc. Aust. Physiol. Soc.* **43,** 65P (abstr.)
30. Schnölzer, M., Alewood, P., Jones, A., Alewood, D., and Kent, S. B. (1992) *In situ* neutralization in Boc-chemistry solid phase peptide synthesis. *Int. J. Pept. Protein Res.* **40,** 180–193
31. Clark, R. J., Daly, N. L., and Craik, D. J. (2006) Structural plasticity of the cyclic-cystine-knot framework. Implications for biological activity and drug design. *Biochem. J.* **394,** 85–93
32. Goddard, T. D., and Kneller, D. G. (2008) SPARKY 3. University of California, San Francisco
33. Rogers, J. P., Luginbühl, P., Shen, G. S., McCabe, R. T., Stevens, R. C., and Wemmer, D. E. (1999) NMR solution structure of α-conotoxin ImI and comparison to other conotoxins specific for neuronal nicotinic acetylcholine receptors. *Biochemistry* **38,** 3874–3882
34. Gehrmann, J., Daly, N. L., Alewood, P. F., and Craik, D. J. (1999) Solution structure of α-conotoxin ImI by ^1H nuclear magnetic resonance. *J. Med. Chem.* **42,** 2364–2372
35. Halai, R., Clark, R. J., Nevin, S. T., Jensen, J. E., Adams, D. J., and Craik, D. J. (2009) Scanning mutagenesis of α-conotoxin Vc1.1 reveals residues crucial for activity at the α9α10 nicotinic acetylcholine receptor. *J. Biol. Chem.* **284,** 20275–20284
36. Wishart, D. S., Bigam, C. G., Holm, A., Hodges, R. S., and Sykes, B. D. (1995) ^1H, ^{13}C, and ^{15}N random coil NMR chemical shifts of the common amino acids. I. Investigations of nearest-neighbor effects. *J. Biomol. NMR* **5,** 67–81
37. Marx, U. C., Daly, N. L., and Craik, D. J. (2006) NMR of conotoxins. Structural features and an analysis of chemical shifts of post-translationally modified amino acids. *Magn. Reson. Chem.* **44,** S41–S50
38. Dougherty, D. A. (2013) The cation-π interaction. *Acc. Chem. Res.* **46,** 885–893
39. Gallivan, J. P., and Dougherty, D. A. (1999) Cation-π interactions in structural biology. *Proc. Natl. Acad. Sci. U.S.A.* **96,** 9459–9464
40. Samanta, U., Pal, D., and Chakrabarti, P. (1999) Packing of aromatic rings against tryptophan residues in proteins. *Acta Crystallogr. D. Biol. Crystallogr.* **55,** 1421–1427
41. van Lierop, B. J., Robinson, S. D., Kompella, S. N., Belgi, A., McArthur, J. R., Hung, A., Macraild, C. A., Adams, D. J., Norton, R. S., and Robinson, A. J. (2013) Dicarba α-conotoxin Vc1.1 analogues with differential selectivity for nicotinic acetylcholine and $GABA_B$ receptors. *ACS Chem. Biol.* **8,** 1815–1821
42. Morris, G. M., Huey, R., Lindstrom, W., Sanner, M. F., Belew, R. K., Goodsell, D. S., and Olson, A. J. (2009) AutoDock4 and AutoDockTools4. Automated docking with selective receptor flexibility. *J. Comput. Chem.* **30,** 2785–2791
43. Kapono, C. A., Thapa, P., Cabalteja, C. C., Guendisch, D., Collier, A. C., and Bingham, J. P. (2013) Conotoxin truncation as a post-translational modification to increase the pharmacological diversity within the milked venom of *Conus magus*. *Toxicon* **70,** 170–178
44. Inserra, M. C., Kompella, S. N., Vetter, I., Brust, A., Daly, N. L., Cuny, H., Craik, D. J., Alewood, P. F., Adams, D. J., and Lewis, R. J. (2013) Isolation and characterization of α-conotoxin LsIA with potent activity at nicotinic acetylcholine receptors. *Biochem. Pharmacol.* **86,** 791–799
45. Taly, A., Corringer, P. J., Guedin, D., Lestage, P., and Changeux, J. P. (2009) Nicotinic receptors. Allosteric transitions and therapeutic targets in the nervous system. *Nat. Rev. Drug Discov.* **8,** 733–750
46. Rucktooa, P., Smit, A. B., and Sixma, T. K. (2009) Insight in nAChR subtype selectivity from AChBP crystal structures. *Biochem. Pharmacol.* **78,** 777–787
47. Hansen, S. B., Sulzenbacher, G., Huxford, T., Marchot, P., Taylor, P., and Bourne, Y. (2005) Structures of *Aplysia* AChBP complexes with nicotinic agonists and antagonists reveal distinctive binding interfaces and conformations. *EMBO J.* **24,** 3635–3646
48. Celie, P. H., Kasheverov, I. E., Mordvintsev, D. Y., Hogg, R. C., van Nierop, P., van Elk, R., van Rossum-Fikkert, S. E., Zhmak, M. N., Bertrand, D., Tsetlin, V., Sixma, T. K., and Smit, A. B. (2005) Crystal structure of nicotinic acetylcholine receptor homolog AChBP in complex with an α-conotoxin PnIA variant. *Nat. Struct. Mol. Biol.* **12,** 582–588
49. Ulens, C., Hogg, R. C., Celie, P. H., Bertrand, D., Tsetlin, V., Smit, A. B., and Sixma, T. K. (2006) Structural determinants of selective α-conotoxin binding to a nicotinic acetylcholine receptor homolog AChBP. *Proc. Natl. Acad. Sci. U.S.A.* **103,** 3615–3620
50. Yu, R., Craik, D. J., and Kaas, Q. (2011) Blockade of neuronal α7-nAChR by α-conotoxin ImI explained by computational scanning and energy calculations. *PLoS Comput. Biol.* **7,** e1002011
51. Lee, C., Lee, S. H., Kim, D. H., and Han, K. H. (2012) Molecular docking study on the α3β2 neuronal nicotinic acetylcholine receptor complexed with α-conotoxin GIC. *BMB Rep.* **45,** 275–280
52. Dutertre, S., Nicke, A., and Lewis, R. J. (2005) β2 subunit contribution to 4/7 α-conotoxin binding to the nicotinic acetylcholine receptor. *J. Biol. Chem.* **280,** 30460–30468
53. Quiram, P. A., Jones, J. J., and Sine, S. M. (1999) Pairwise interactions between neuronal α7 acetylcholine receptors and α-conotoxin ImI. *J. Biol. Chem.* **274,** 19517–19524
54. Young, G. T., Broad, L. M., Zwart, R., Astles, P. C., Bodkin, M., Sher, E., and Millar, N. S. (2007) Species selectivity of a nicotinic acetylcholine receptor agonist is conferred by two adjacent extracellular β4 amino acids that are implicated in the coupling of binding to channel gating. *Mol. Pharmacol.* **71,** 389–397

55. Parker, M. J., Harvey, S. C., and Luetje, C. W. (2001) Determinants of agonist binding affinity on neuronal nicotinic receptor β subunits. *J. Pharmacol. Exp. Ther.* **299,** 385–391
56. Harvey, S. C., and Luetje, C. W. (1996) Determinants of competitive antagonist sensitivity on neuronal nicotinic receptor β subunits. *J. Neurosci.* **16,** 3798–3806
57. Shimomura, M., Yokota, M., Ihara, M., Akamatsu, M., Sattelle, D. B., and Matsuda, K. (2006) Role in the selectivity of neonicotinoids of insect-specific basic residues in loop D of the nicotinic acetylcholine receptor agonist binding site. *Mol. Pharmacol.* **70,** 1255–1263
58. Harvey, S. C., McIntosh, J. M., Cartier, G. E., Maddox, F. N., and Luetje, C. W. (1997) Determinants of specificity for α-conotoxin MII on α3β2 neuronal nicotinic receptors. *Mol. Pharmacol.* **51,** 336–342
59. Shiembob, D. L., Roberts, R. L., Luetje, C. W., and McIntosh, J. M. (2006) Determinants of α-conotoxin BuIA selectivity on the nicotinic acetylcholine receptor β subunit. *Biochemistry* **45,** 11200–11207
60. Brams, M., Gay, E. A., Sáez, J. C., Guskov, A., van Elk, R., van der Schors, R. C., Peigneur, S., Tytgat, J., Strelkov, S. V., Smit, A. B., Yakel, J. L., and Ulens, C. (2011) Crystal structures of a cysteine-modified mutant in loop D of acetylcholine-binding protein. *J. Biol. Chem.* **286,** 4420–4428
61. Xie, Y., and Cohen, J. B. (2001) Contributions of Torpedo nicotinic acetylcholine receptor γ Trp-55 and δ Trp-57 to agonist and competitive antagonist function. *J. Biol. Chem.* **276,** 2417–2426
62. Williams, D. K., Stokes, C., Horenstein, N. A., and Papke, R. L. (2009) Differential regulation of receptor activation and agonist selectivity by highly conserved tryptophans in the nicotinic acetylcholine receptor binding site. *J. Pharmacol. Exp. Ther.* **330,** 40–53
63. Billen, B., Spurny, R., Brams, M., van Elk, R., Valera-Kummer, S., Yakel, J. L., Voets, T., Bertrand, D., Smit, A. B., and Ulens, C. (2012) Molecular actions of smoking cessation drugs at α4β2 nicotinic receptors defined in crystal structures of a homologous binding protein. *Proc. Natl. Acad. Sci. U.S.A.* **109,** 9173–9178
64. Gay, E. A., Bienstock, R. J., Lamb, P. W., and Yakel, J. L. (2007) Structural determinates for apolipoprotein E-derived peptide interaction with the α7 nicotinic acetylcholine receptor. *Mol. Pharmacol.* **72,** 838–849
65. Hansen, S. B., and Taylor, P. (2007) Galanthamine and non-competitive inhibitor binding to ACh-binding protein. Evidence for a binding site on non-α-subunit interfaces of heteromeric neuronal nicotinic receptors. *J. Mol. Biol.* **369,** 895–901
66. Seo, S., Henry, J. T., Lewis, A. H., Wang, N., and Levandoski, M. M. (2009) The positive allosteric modulator morantel binds at noncanonical subunit interfaces of neuronal nicotinic acetylcholine receptors. *J. Neurosci.* **29,** 8734–8742
67. Yu, R., Kompella, S. N., Adams, D. J., Craik, D. J., and Kaas, Q. (2013) Determination of the α-conotoxin Vc1.1 binding bite on the α9α10 nicotinic acetylcholine receptor. *J. Med. Chem.* **56,** 3557–3567
68. Xiu, X., Puskar, N. L., Shanata, J. A., Lester, H. A., and Dougherty, D. A. (2009) Nicotine binding to brain receptors requires a strong cation-π interaction. *Nature* **458,** 534–537
69. Puskar, N. L., Xiu, X., Lester, H. A., and Dougherty, D. A. (2011) Two neuronal nicotinic acetylcholine receptors, α4β4 and α7, show differential agonist binding modes. *J. Biol. Chem.* **286,** 14618–14627
70. Wu, J., Kuo, Y. P., George, A. A., Xu, L., Hu, J., and Lukas, R. J. (2004) β-Amyloid directly inhibits human α4β2-nicotinic acetylcholine receptors heterologously expressed in human SH-EP1 cells. *J. Biol. Chem.* **279,** 37842–37851
71. Gay, E. A., Giniatullin, R., Skorinkin, A., and Yakel, J. L. (2008) Aromatic residues at position 55 of rat α7 nicotinic acetylcholine receptors are critical for maintaining rapid desensitization. *J. Physiol.* **586,** 1105–1115
72. Hibbs, R. E., Sulzenbacher, G., Shi, J., Talley, T. T., Conrod, S., Kem, W. R., Taylor, P., Marchot, P., and Bourne, Y. (2009) Structural determinants for interaction of partial agonists with acetylcholine binding protein and neuronal α7 nicotinic acetylcholine receptor. *EMBO J.* **28,** 3040–3051
73. Lester, H. A., Dibas, M. I., Dahan, D. S., Leite, J. F., and Dougherty, D. A. (2004) Cys-loop receptors. New twists and turns. *Trends Neurosci.* **27,** 329–336
74. Kesters, D., Thompson, A. J., Brams, M., van Elk, R., Spurny, R., Geitmann, M., Villalgordo, J. M., Guskov, A., Danielson, U. H., Lummis, S. C., Smit, A. B., and Ulens, C. (2013) Structural basis of ligand recognition in 5-HT_3 receptors. *EMBO Rep.* **14,** 49–56
75. Van der Spoel, D., Lindahl, E., Hess, B., Groenhof, G., Mark, A. E., and Berendsen, H. J. C. (2005) GROMACS: Fast, flexible, and free. *J. Comput. Chem.* **26,** 1701–1718
76. MacKerell, A. D., Brooks, C. L., Nilsson, L., Roux, B., Won, Y., and Karplus, M. (1998) in *The Encyclopedia of Computational Chemistry* (Schleyer, P., ed) Vol. 1, p. 271, John Wiley & Sons, Chichester
77. Bjelkmar, P., Larsson, P., Cuendet, M. A., Hess, B., and Lindahl, E. (2010) Implementation of the CHARMM force field in GROMACS: Analysis of protein stability effects from correction maps, virtual interaction sites, and water models. *J. Chem. Theory Comput.* **6,** 459–466
78. Humphrey, W., Dalke, A., and Schulten, K. (1996) VMD—Visual Molecular Dynamics. *J. Mol. Graphics* **14,** 33–38

Identifying Key Amino Acid Residues That Affect α-Conotoxin AuIB Inhibition of α3β4 Nicotinic Acetylcholine Receptors

Anton A. Grishin, Hartmut Cuny, Andrew Hung, Richard J. Clark, Andreas Brust, Kalyana Akondi, Paul F. Alewood, David J. Craik and David J. Adams

J. Biol. Chem. 2013, 288:34428-34442.
doi: 10.1074/jbc.M113.512582 originally published online October 7, 2013
